Hyperpolarized Xenon Brain MRI

Xin Zhou
Wuhan Center for Magnetic Resonance,
State Key Laboratory of Magnetic Resonance and Atomic and Molecular Physics,
Wuhan Institute of Physics and Mathematics,
The Chinese Academy of Sciences, Wuhan,
P.R. China

1. Introduction

Since hyperpolarized ^{129}Xe MRI was first demonstrated in the lung, air space imaging using hyperpolarized noble gases (^{129}Xe and ^{3}He) has progressed at a rapid rate (Goodson, 2002; Zhou, 2011c). Owing to high lipid solubility, absence of background signal in biological tissue, non-invasiveness, lack of radioactivity, different relaxation to oxygenated and deoxygenated blood, and larger chemical shift to the neighbor environment, hyperpolarized ^{129}Xe magnetic resonance imaging (MRI) has a great potential as a tool for studying the brain, especially for the assessment of cerebral blood flow (CBF) related to the brain function and activities.

In this chapter, we will review the progress of recent research on hyperpolarized xenon brain MRI, and compare this novel technique with the conventional proton MRI in order to comment the possible innovation and development in the future. This chapter contains six main parts as follows:

2. Properties of xenon

Xenon, with the chemical element symbol Xe and atomic number 54, is a member of the zero-valence elements that are called noble gases or inert gases. Xenon was discovered in the residue left over from evaporating components of liquid air by William Ramsay and Morris Travers in England in 1898, then was named by Ramsay from Greek word *ξένον*, with the meaning 'foreign' and 'strange'. Natural abundant xenon is made of nine stable isotopes, and more than 35 unstable isotopes have been characterized. Nuclei of two isotopes, ^{129}Xe and ^{131}Xe, have non-zero spin quantum number: 26.4% of ^{129}Xe with a nuclear spin I=1/2 ; and 21.2% of ^{131}Xe with a nuclear spin I=3/2 (^{133}Xe is used as a radioisotope in nuclear medicine). These two isotopes are both detectable by NMR with sensitivities of 0.021 (^{129}Xe, per nucleus relative to proton assuming thermal polarization) and 2.7×10^{-3} (^{131}Xe). The highly enhanced signal of hyperpolarized xenon and extremely long relaxation time greatly simplified and enhanced NMR experiments, and it is the fundamental for possible biological application in MRI.

Xenon, chemically inert with the external electronic orbits fully occupied, is well known as a noble gas at room temperature and an atmospheric pressure. However, the liquid and solid

phases of Xenon can be easily obtained within an experimentally accessible range of temperatures and pressures (Cook, 1961) (Fig. 1).
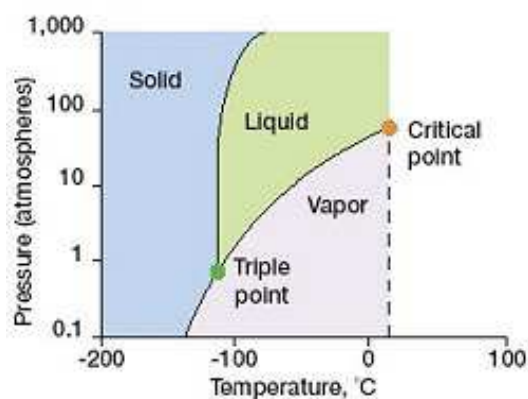

Fig. 1. Phase diagram of xenon.
(Figure from: http://science.nasa.gov/science-news/science-at-nasa/2008/25apr_cvx2/)

Furthermore, the large and highly polarizable electron cloud makes xenon highly lipid soluble in solution, without chemically or structurally damage during interactions with other molecules. Ostwald solubility is defined as the ratio of the volume of the gas absorbed to the volume of the absorbing liquid, measured at same temperature and a pressure of 1 atm (101,325 Pa) (Cherubini, 2003; Oros, 2004) (Table 1).

Compound	Ostwald solubility
T=25 °C	
Water	0.11
Hexane	4.8
Benzene	3.1
Fluorobenzene	3.3
Carbon disulphide	4.2
T=37 °C	
Water	0.08
Saline	0.09
Plasma	0.10
Erythrocytes (98%)	0.20
Human albumin (100%,extrapolated)	0.15
Blood	0.14
Oil	1.9
Fat tissue	1.3
DMSO (dimethyl sulfoxide)	0.66
Intralipid (20%)	0.4
PFOB (perflubron)	1.2
PFOB (90% w/v, estimated)	0.62

Table 1. Solubilities of xenon gas in various compounds. (Data taken from Cherubini, 2003)

Owing to the inter-atomic collisions distortion of xenon electron cloud during the interactions with different chemical environment, the chemical shift of [129]Xe is extremely sensitive. Total solvent effect on the Xe resonance frequency is over 7500 ppm, very large compared with most other NMR sensitive nuclei ([1]H : 20 ppm、[13]C : 300 ppm). A few examples are shown in Figure 2, the natural reference point for xenon chemical shift in the gas phase; with respect to the gas resonance (0 ppm), peaks at 70 ppm corresponding to cryptophane-bound xenon; around 197 ppm, five dissolved peaks can be observed, a dominant peak at 194.7 ppm and another discriminable peak at 189 ppm are identified as dissolved hyperpolarized [129]Xe in the brain tissue and non-brain tissue, respectively, two small peaks at 191.6 ppm and 197.8 ppm are still unknown, and a smaller broad peak at 209.5 ppm comes from the dissolved hyperpolarized [129]Xe in the blood (Zhou et al., 2008).
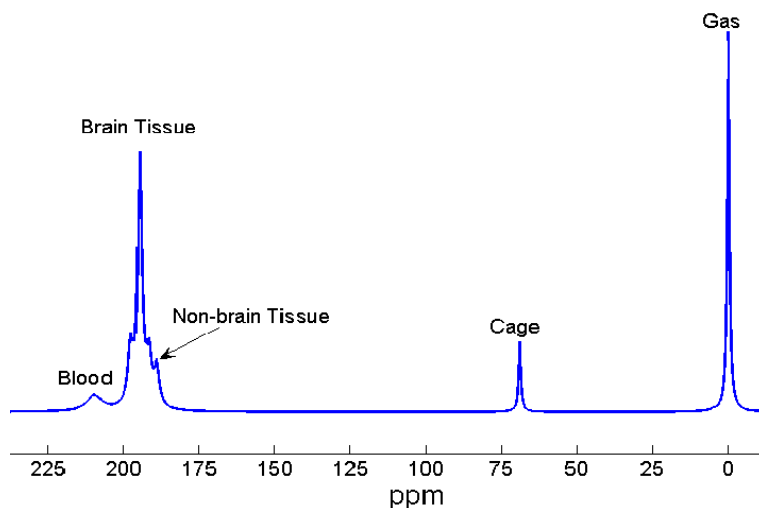

Fig. 2. Chemical shift of [129]Xe in biosensor and biological system (Data taken from Zhou et al., 2011c)

As a closed shelled noble gas, xenon has a peculiar large polarizable electron cloud, it can be easily interacted with biological materials, including water 'lipids' and proteins and so on; meanwhile, [129]Xe NMR parameters like relaxation time and chemical shift are very sensitive to local chemical environment, these biochemical physiological characters make xenon a very interesting NMR probe for biological applications. Arising from large increase in sensitivity associated with hyperpolarized [129]Xe, the biological NMR applications have been dramatically extended. Being Chemically Inert, xenon can be safely delivered into living organisms, associated with another advantage of no background signal, thus *in vivo* MR imaging and spectroscopy is possible using hyperpolarized [129]Xe technique.

3. Signal enhanced MRI with hyperpolarized [129]Xe

Nuclear magnetic resonance (NMR) has been widely used in most fields of natural sciences, such as physics, chemistry, biology, and medicine. Because of the intrinsic low nuclear spin polarization at the thermal equilibrium, NMR is relatively insensitive. The normal [129]Xe MRI, i.e., at the thermal equilibrium, is not able to get enough signal to visualize tissues or organs. The polarization can be moderately increased by using lower temperature or higher

magnetic fields (Navon et al., 1996), whereas the nuclear spin polarizations of noble gases can be increased by four or five orders of magnitude via the spin-exchange optical pumping (SEOP) techniques (Walker, 1997). Therefore, it enables a very high sensitive detection of hyperpolarized ^{129}Xe MRI. This subsection will describe how to produce hyperpolarized ^{129}Xe, which is the basis for the brain imaging.

^{3}He and ^{129}Xe are generally selected for hyperpolarized lung gas imaging, because ^{3}He and ^{129}Xe are the only noble gas nuclei with nuclear spin 1/2, which results in the longitudinal relaxation time of many hours or even days at the standard temperature and pressure. However, hyperpolarized ^{3}He could not be used for the brain study due to the extremely low solubility in blood and tissue, while hyperpolarized ^{129}Xe is a novel contrast agent for the cerebral research. Hyperpolarized ^{129}Xe is generally generated by employing the technique of SEOP.

For SEOP, the first step is to transfer the anglar momentum of the cicularly polarized laser light to the electronic spin, i.e., optical pumping. In principal, any alkali metal vapor can be optically pumped. Rb is normally used as the corresponding pumping laser diode arrays (LDA), which are routinely manufactured in high power configurations. When the Rb vapor experiences an external magnetic field of 20-30 Gauss, the ground state $5^{2}S_{1/2}$ is split into two Zeeman sublevels, M_J=-1/2 and M_J=1/2, i.e., electronic spin "down" or "up". These two Zeeman states have a nearly equal population at room temperature. After the Rb vapor absorbs the circularly polarized laser light (σ+) centered at 795nm, the Rb D1 transition occurs, i.e., $5^{2}S_{1/2} \rightarrow 5^{2}P_{1/2}$. Accordingly, the ground state with a sublevel M_J=-1/2 is pumped into the excited state, M_J=1/2. The nitrogen gas quenches the excited state back to the ground state. Because the M_J=-1/2 sublevel continues to absorb the circularly polarized light (σ+) an excess of Rb atoms are optically pumped into the Zeeman sublevel M_J=1/2 while the other sublevel M_J=-1/2 is depleted. Therefore, an Rb electronic spin polarization of roughly 100% is able to be achieved.

The second step of SEOP is spin exchange, which occurs between the polarized electronic spins of Rb and the xenon nucleus. The collision between polarized Rb atoms and xenon atoms induces the transfer of angular momentum from the electronic spin to the nuclear spin. During this collision, the electron wave function of the Rb overlaps the nuclear wave function of xenon, which results in the spin exchange between the electronic spin and nuclear spin. Binary collisions dominate the spin exchange at high pressure, while three-body collision (by forming a Rb/Xe van der Waals molecule) dominate at low pressure (a few tens of torr).

Generally, Rb atoms and nitrogen gas are employed for optical pumping, however, Cs may be proposed as a better candidate for spin exchange with ^{129}Xe due to several advantages: the natural abundance of ^{133}Cs is 100% while Rb has two isotopes (^{85}Rb and ^{87}Rb), so that Cs is more convenient than Rb for wide applications of hyperpolarized ^{129}Xe, particularly in the clinic application; optical pumping cells for Cs are operated at lower temperatures with correspondingly fewer chemical corrosion problems; according to the previous experimental results, the spin-exchange rate of Cs-Xe is about 10% higher than the Rb-Xe rate (Zhou et al., 2004a). When the polarization of hyperpolarized ^{129}Xe is high enough, the observed radiation damping has been reported (Zhou, 2004b). The xenon polarizer with a flow feature can be readily extended to produce larger quantities of hyperpolarized ^{129}Xe for not only medical imaging but also materials science and biology (Zhou, 2004c; Zhou, 2009a).

4. Longitudinal relaxation time (T$_1$) of hyperpolarized ^{129}Xe in the brain

Hyperpolarized ^{129}Xe magnetization enhanced by SEOP is non-recoverable, and the T$_1$ of an hyperpolarized gas is the time elapsed for the signal to decay, because its thermal equilibrium polarization is almost zero relative to the hyperpolarized polarization. Usually, small flip angles has to be used to ration the hyperpolarized magnetization, and it is very important to have a T$_1$ as long as possible to ensure that the signal lasts long enough for the acquisition. Therefore, the T$_1$ of hyperpolarized ^{129}Xe in the brain is a critical parameter. This subsection will discuss the aspects that affect T$_1$ of hyperpolarized xenon, and describe the methods to accurately measure the T$_1$ in the brain (Zhou et. al, 2008).

4.1 T$_1$ of hyperpolarized ^{129}Xe

For conventional MRI, the magnetization at thermal equilibrium is induced by the magnetic field, and the longitudinal relaxation time (T$_1$) is the time for the magnetization, i.e. the magnetic resonance signal, to recover back to the thermal equilibrium. However, hyperpolarized noble gas magnetization produced by SEOP is unable to recover back to the hyperpolarized magnetization by itself, and the T$_1$ of an hyperpolarized noble gas is the decay time of magnetization, because the thermal polarized magnetization is almost zero related to the hyperpolarized magnetization. The longitudinal relaxation time of hyperpolarized ^{129}Xe in the brain is a critical parameter for developing hyperpolarized ^{129}Xe brain imaging and spectroscopy and optimizing the pulse sequences, especially in the case of cerebral blood flow measurements. Various studies have produced widely varying estimates of hyperpolarized ^{129}Xe T$_1$ in the rat brain (Choquet, 2003; Wakai, 2005).

The hyperpolarized magnetization is generally tipped by a pulse with a small flip angle, and it is very challenging to make the T$_1$ as long as possible in order to ensure the signal lasts long enough for the acquisition. Therefore, when considering hyperpolarized ^{129}Xe as a marker for brain perfusion by MRI, evaluation of tissue characterization and pulse sequence optimization, the T$_1$ of hyperpolarized ^{129}Xe in the brain is a critical parameter. Previous attempts to measure T$_1$ in the rat brain have yielded strikingly disparate results. Wilson et al. found that T$_1$ measured in rat brain homogenates in vitro ranged from 18±1 to 22±2 s (mean ± SD) (Wilson et. al，2009) depending on the oxygenation level of the tissue, and T$_1$ values from measurements in rat brain *in vivo* have ranged from 3.6±2.1 (Choquet et al, 2003) to 26±4 s (Wakai et. al, 2005). Part of the discrepancy is believed to be due to the protocols used in T$_1$ determination. The attempt of Choquet et al. used a multi-pulse protocol during the uptake and washout process by injecting hyperpolarized ^{129}Xe in a lipid emulsion, whereas the estimation of Wakai et al. used a two-pulse protocol during the washout process after the rat had breathed hyperpolarized ^{129}Xe gas. Under the condition of typically achieved polarizations (5–21%) (Zook et. al, 2001), low signal-to-noise ratio (SNR) due to the low concentration of the dissolved hyperpolarized ^{129}Xe in tissue is an important factor in making T$_1$ measurements in the rat brain (Cherubinia et. al, 2003; Ruppert et. al, 2000). The maximum SNR in the above two measurements in vivo was only 30 (Choquet et. al, 2003) and 46 (Wakai et. al, 2005), and the noise effect was not considered in these studies. When the SNR is low, noise will dominate the measured signal and result in large differences between the true T$_1$ and the measured T$_1$. Thus, low SNR might be a large contributor of error in the published T$_1$ values.

4.2 Multi-pulse and two-pulse washout protocols for measurements of T_1

Hyperpolarized ^{129}Xe transport in the brain has been modeled using appropriate adaptations of the Kety–Schmidt theory (Martin et al., 1997; Peled et al., 1996). Martin and co-workers derived the equation of the cerebral xenon concentration during hyperpolarized ^{129}Xe delivery to the lungs as follow:

$$\frac{dC_{brain}}{dt} = FC_{cereb} - \left(\frac{F}{p} + \frac{1}{T_{1brain}}\right)C_{brain} \tag{1}$$

where C_{cereb} is the xenon concentration in the cerebral artery, C_{brain} is the xenon concentration in brain parenchyma, F is the tissue perfusion in units of (volume blood)/(volume tissue)/time, p is the brain/blood partition coefficient for xenon, and T_{1brain} is the longitudinal relaxation time of xenon in the brain. In this equation, the first term on the right describes xenon transport to the brain, and the second term describes the loss of xenon signal due to both perfusion and T_1 decay. Xenon signal observed from the brain is proportional to C_{brain}. During the washout phase of the xenon signal, there is no transport of hyperpolarized ^{129}Xe by the cerebral artery, and hence C_{cereb} is zero. Accordingly, the xenon concentration in the brain during washout ($C_{brainwashout}$) is given by the following equation:

$$\frac{dC_{brainwashout}}{dt} = -\left(\frac{F}{p} + \frac{1}{T_{1brain}}\right)C_{brainwashout} \tag{2}$$

This equation can be solved to yield an analytical solution for the concentration of xenon in the brain during the washout of signal. The decay time constant (τ) of hyperpolarized ^{129}Xe during the washout from the rat brain is given by:

$$\tau = \frac{1}{\left(\frac{F}{p} + \frac{1}{T_{1brain}}\right)} \tag{3}$$

Thus, τ can be calculated from a series of pulse excitations (multi-pulse protocol) after compensating for the hyperpolarized xenon signal losses resulted from radio frequency (RF) excitation, as described below. To compare the results obtained using the multi-pulse protocol, a two-pulse protocol has also been adopted to measure τ (Wakai et al., 2005). Both protocols were performed on each rat during the washout phase of the ^{129}Xe signal.

Table 2 shows individual T_1 values of hyperpolarized ^{129}Xe and their mean from the six rat brains using the two protocols, with and without the SNR threshold. The mean T_1 value calculated using the improved two-pulse method is larger than that using its conventional counterpart, whereas the mean T_1 value calculated using the improved multi-pulse method is less than that using its conventional counterpart. These T_1 values were named 'group 1' to 'group 4' for easy reference during discussion.

In this subsection, we investigated the error in T_1 measurement as a result of low SNR of the ^{129}Xe signal *in vivo*. Correcting for these errors allowed us to more accurately measure the T_1 of hyperpolarized ^{129}Xe in the rat brain *in vivo*. Our calculations produced highly consistent

T_1 results independent of the measurement protocol and offer a resolution to the discrepancy between previously reported values.

Rat	Multi-pulse protocol		2-pulse protocol	
	Conventional	Improved	Conventional	Improved
	$T_1(s)$ (group 1)	$T_1(s)$ (group 2)	$T_1(s)$ (group 3)	$T_1(s)$ (group 4)
1	14.2	12.9	19.5	17.6
2	12.2	15.1	18.2	16.4
3	11.5	16.1	16.3	14.9
4	11.7	15.5	18.0	16.5
5	12.7	16.4	18.8	16.6
6	12.1	15.7	17.2	15.4
Mean	12.4	15.3	18.0	16.2
Std. Deviation	1.0	1.2	1.1	0.9

Table 2. T_1 values of hyperpolarized [129]Xe from six rat brains. The mean T_1 value and standard deviation obtained from the multi-pulse and two-pulse protocols before (conventional method) and after (improved method) setting a threshold of SNR=5.5 are also given. (Zhou et al., 2008)

5. Stroke MRI with hyperpolarized [129]Xe

Because there is no background signal from xenon in biological tissue, and because the inhaled xenon is delivered to the brain by the blood flow, we would expect a perfusion deficit, such as could be seen in stroke, to reduce xenon concentration in the region of the deficit. Thermal polarization yields negligible xenon signal relative to hyperpolarized xenon; therefore, hyperpolarized xenon can be used as a tracer of cerebral blood flow (CBF). This subsection will describe that hyperpolarized [129]Xe MRI is able to detect, *in vivo* hypoperfused area of focal cerebral ischemia—i.e., the ischemic core area of stroke, by using a rat permanent right middle cerebral artery occlusion (MCAO) model (Zhou et al., 2011a).

Stroke is the single most common reason for permanent disability and is the third leading cause of death in developed countries. During acute ischemic stroke, a core of brain cells at the center of the affected region dies quickly, and the damage subsequently spreads to surrounding tissue over the next few hours. Because they allow for the delineation of areas of ischemic neuronal injury and hypoperfusion within minutes after the induction of cerebral ischemia, conventional proton MRI, especially diffusion-weighted imaging (DWI) and perfusion weighted imaging (PWI), have been particularly useful in the diagnosis of acute ischemic stroke. The target of acute stroke therapy is the portion of the ischemic region

which is still potentially salvageable, that is the ischemic penumbra. MRI operationally defines the ischemic penumbra by the mismatch area of PWI–DWI. DWI detects changes in the apparent diffusion coefficient (ADC) of water molecules associated with early cytotoxic edema in ischemic stroke. Arterial spin labeling (ASL)-based PWI methods provide excellent anatomical information for the measurement of tissue perfusion. The ASL technique shows numerous advantages, such as noninvasive measurements of cerebral blood flow (CBF) quantifiable in standard units of mL/g/min, and is able to image multi-slices and multi-regions of the brain. However, in some situations, PWI methods require the injection of gadolinium containing contrast agents to map relative CBF in order to identify the hypoperfused tissue. In addition to the conventional DWI and PWI techniques, van Zijl and coworkers have developed pH-weighted MRI to study stroke and ischemic penumbra. However, proton imaging has a large background signal in biological tissue, and contrast injection is an invasive approach. Moreover, contrast-associated nephrogenic systemic fibrosis has been reported after the use of gadolinium-based agents, and many patients with impaired renal function are not eligible to receive contrast media. In contrast, hyperpolarized [129]Xe MRI shows great potential and advantages for the identification of hypoperfused brain tissue. Xenon is highly lipid soluble and lacks an intrinsic background signal in biological tissue (Albert et al., 1994). Duhamel and co-workers have studied CBF using intra-arterial injection of hyperpolarized [129]Xe dissolved in a lipid emulsion (Duhamel et al., 2000). Alternatively, hyperpolarized [129]Xe can be administered noninvasively by inhalation; following inhalation, [129]Xe is absorbed into the bloodstream and delivered to the brain through the circulation. Because the spin-exchange optical pumping technique can enhance the [129]Xe MR signal 10,000–100,000 times over thermal polarization, the dissolved-phase hyperpolarized [129]Xe signal in the brain can be detected even at low concentrations. Because the xenon signal is proportional to CBF (Zhou et al., 2008), a decrease in the signal is expected to occur in areas of decreased CBF after the inhalation of hyperpolarized xenon gas. Hyperpolarized xenon imaging currently can not achieve a slice as thin as that obtained by ASL. In addition, ASL can be performed with substantially higher spatial resolution than hyperpolarized xenon imaging in brain tissue. However, the ASL technique requires two experiments (arterial spin labeled and controlled) to obtain CBF information. In this subsection, we report, for the first time, that hyperpolarized [129]Xe MRI is able to detect areas of decreased CBF following middle cerebral artery occlusion (MCAO) in a single scan. These findings show the great potential and utility of hyperpolarized [129]Xe MRI for stroke imaging, and further demonstrate that hyperpolarized [129]Xe is a safe and noninvasive signal source for imaging diseases and function of the brain.

Figure 3a shows a representative proton ADC map obtained 90 min following MCAO. There is a large ischemic core within the ipsilesional (right) MCA territory, as indicated by ADC values below the critical threshold of 5.3×10^{-4} mm^2/s for infarction (Meng et al., 2004). [The normal ADC value of rat brain tissue in the contralesional (left) hemisphere is $(7.5\pm1.8)\times10^{-4}$ mm^2/s.] Figure 3b depicts the corresponding hyperpolarized [129]Xe CSI, indicating signal reduction in large parts of the right hemisphere, consistent with the area typically experiencing decreased CBF following right MCAO in the model used (Duhamel et al., 2002). Figure 3c shows the TTC-stained brain section of the same animal as illustrated in Fig. 3a, b; the black line in this figure delineates the infracted brain tissue. Xenon CSI, shown in Fig. 3b, demonstrates reduced perfusion in brain tissue, ultimately leading to infarction, as shown by TTC staining in Fig. 3c. In Fig. 3d, the blue area represents the difference between

the ADC lesion and TTC lesion areas, and the green area shows the nonischemic region. ROI analyses were performed to further characterize the Xe CSI tissue signals within the different observed tissue compartments defined by their respective ADC and TTC signatures.

Xenon signals from each ROI in the contralesional (left) hemisphere were set as a reference (100%), and xenon signals from each ROI in the ipsilesional (right) hemisphere were normalized to these signals. The xenon signal in the ischemic core (ROI_1) dropped to $8.4\pm0.4\%$ of the contralesional side signal, and the xenon signal in normal tissue (ROI_2) remained the same. Moreover, the xenon signal in ROI_1 was reduced significantly relative to the corresponding con-tralesional ROIs in the MCAO group, as well as the corresponding ipsilateral ROIs in control animals. Within the control group, no significant differences in the xenon signal were observed between the corresponding ROIs of both hemispheres.
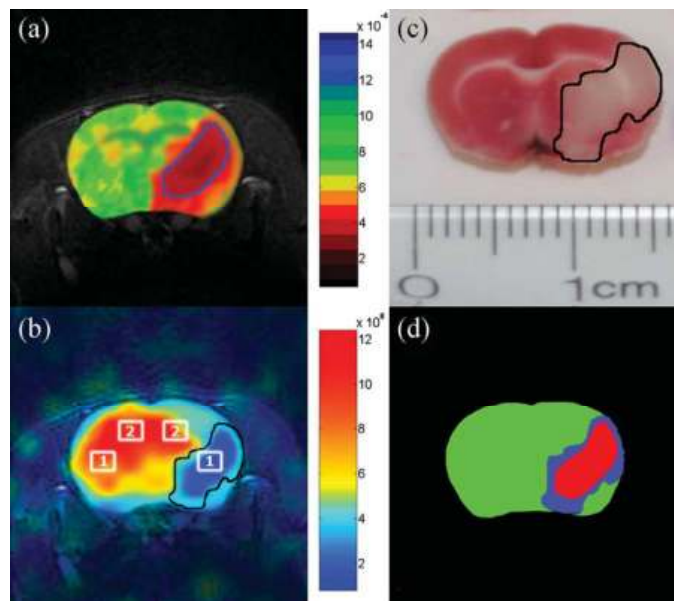

Fig. 3. (a) Representative proton apparent diffusion coefficient (ADC) map image obtained 90 min after right middle cerebral artery occlusion (MCAO). The ischemic core is indicated by ADC values below 5.3×10^{-4} mm^2/s (circled by a blue line). (b) Corresponding hyperpolarized ^{129}Xe chemical shift image (CSI). There is a large signal void in the ipsilesional (right) hemisphere. The defined regions of interest (ROIs) are labeled as follows: ROI1, core; ROI2, normal tissue. The xenon signal intensity is given in arbitrary units. (c) Corresponding 2,3,5-triphenyltetrazolium chloride (TTC)-stained brain section of the same animal as in (a) and (b). (d) Tricolor map based on the ADC and TTC images shown in (a) and (c). Green, red and blue represent nonischemic tissue, core and penumbra, respectively.

Using a rat permanent right middle cerebral artery occlusion model, it has demonstrated that hyperpolarized ^{129}Xe MRI is able to detect, *in vivo*, the hypoperfused area of focal cerebral ischemia, that is the ischemic core area of stroke. To the best of our knowledge, this is the first time that hyperpolarized ^{129}Xe MRI has been used to explore normal and abnormal cerebral perfusion. The study shows a novel application of hyperpolarized ^{129}Xe

MRI for imaging stroke, and further demonstrates its capacity to serve as a complementary tool to proton MRI for the study of the pathophysiology during brain hypoperfusion. More importantly, these results indicate the possibility of the use of *in vivo* MRI to diagnose brain disease employing inhaled hyperpolarized gas, eliminating the potential adverse effects to the patient resulting from the injection of gadolinium-based contrast agents.

6. Functional MRI with hyperpolarized ^{129}Xe

As hyperpolarized xenon is a MRI signal source with properties very different from those generated from water-protons, hyperpolarized ^{129}Xe MRI may yield structural and functional information not detectable by conventional proton-based MRI methods. This subsection shows that the differential distribution of hyperpolarized ^{129}Xe in the cerebral cortex of the rat following a pain stimulus evoked in the animal's forepaw. Areas of higher hyperpolarized ^{129}Xe signal corresponded to those areas previously demonstrated by conventional functional MRI (fMRI) methods as being activated by a forepaw pain stimulus. It demonstrated that the percent increase in hyperpolarized ^{129}Xe signal over baseline was 13 - 28%, which is more sensitive than the conventional fMRI based on the blood oxygen level dependence (BOLD) (2-4%) (Zhou et al., 2011b).

Ex-vivo hyperpolarization of ^{129}Xe is detectable by magnetic resonance spectroscopy (MRS) and MRI in animals and humans, although the resulting *in vivo* signal to noise ratio (SNR) of the hyperpolarized ^{129}Xe signal is not as great as the signal produced by protons in conventional MRI, hyperpolarized ^{129}Xe has several unique characteristics which may endow it with advantages in some imaging applications, including brain imaging (Zhou et.al, 2011a). The nuclear magnetic resonance frequency range (chemical shift) of hyperpolarized ^{129}Xe *in vivo* is large compared to protons (200 ppm vs. 5 ppm respectively) and is also substantially affected by the local chemical environment, providing a means to detect localized physiological changes and biochemical binding events. In particular, the chemical shift experienced by ^{129}Xe in the presence of oxygen (O_2) is substantial and may offer a means to image changes in tissue O_2 concentration that result from changes in neuronal activity. Xenon is also an ideal perfusion tracer (Betz, 1972) and inhaled non-radioactive xenon gas has been used to detect disease induced alterations in cerebral blood flow with high anatomical specificity (Gur, 1982). Because xenon is not intrinsic to biological tissue, hyperpolarized ^{129}Xe produces virtually no background signal, which, in turn, results in high contrast hyperpolarized ^{129}Xe MR images (Swanson, 1997).

6.1 Rat brain functional hyperpolarized ^{129}Xe imaging experiment

In the rat brain function study, hyperpolarized ^{129}Xe MRI was performed in rats to investigate the distribution of the hyperpolarized ^{129}Xe signal following a well-established paradigm for producing anatomically localized neuronal activity. Six rats were intubated and connected to a ventilator that controlled the delivery of oxygen and hyperpolarized ^{129}Xe gas. Male Spragur-Dawley rats weighing between 200-250g were placed on animal respirator, with tidal volume of 3ml O_2 (3% isoflurane included) supplied for each breath. Immediately prior to the acquisition of CSI images, the animal was ventilated with alternate breaths of 100% hyperpolarized ^{129}Xe and 98% O_2: 2% isoflurane. The breath-hold period during the delivery of each hyperpolarized ^{129}Xe breath was 2 seconds.

High resolution proton images were taken of the rat head to provide an anatomical reference for hyperpolarized ^{129}Xe images. In order to evaluate the distribution of hyperpolarized ^{129}Xe in brain following an external sensory stimulus, we acquired MRS images before and after a pain producing stimulus that has a well-defined functional response that can be measured using traditional fMRI techniques. A baseline hyperpolarized ^{129}Xe spectroscopic image was acquired from a coronal slice centered at the level of the anatomical reference slice.

The maximal, steady-state ^{129}Xe brain signal occurred within 15 seconds after starting the ventilation with hyperpolarized ^{129}Xe. Once verification of the xenon signal in the brain, a baseline ^{129}Xe chemical shift image (CSI) was acquired that was centred in the plane corresponding to the proton reference image. Low flip angle used for CSI acquisition insured minimal loss of hyperpolarized ^{129}Xe signal due to RF destruction, and the relatively long TR allowed continuous delivery of hyperpolarized ^{129}Xe to the tissue, a steady–state concentration of hyperpolarized ^{129}Xe was maintained in the brain thereby insuring constant signal intensity across the k-space. In a subset of animals (n=3) the animal's left forepaw was injected with a vehicle solution during baseline. Following acquisition of the baseline CSI image, the animal was ventilated for 10 minutes with O_2 (isoflurane to allow for complete clearance of ^{129}Xe magnetization from the brain). After that, the chemical irritant capsaicin (20 ul of 3 mg/ml) was injected into the animal's right forepaw (n= 6), and a second CSI was acquired.

6.2 Experiment results and discussion

A robust hyperpolarized ^{129}Xe spectroscopic signal with one primary peak at 194.7 ppm developed within 15 seconds after starting the ventilation with hyperpolarized ^{129}Xe. In order to determine the extent of hyperpolarized ^{129}Xe distribution throughout the rat brain, a magnetic resonance spectroscopic image was acquired of the primary peak during the administration of hyperpolarized ^{129}Xe (Figure 4). The four smaller resonances did not have sufficient SNR to produce spectroscopic images. Figure 4a shows an hyperpolarized ^{129}Xe image taken in the axial plane. Addition of a color look-up table (Figure 4b) aided in visually delineating areas of low and high SNR. Figure 4c show a 1 mm proton slice in which the olfactory bulbs and cerebellum are visible. Overlay of the hyperpolarized ^{129}Xe spectroscopic image onto the proton reference image (Figure 4d) revealed that the steady-state hyperpolarized ^{129}Xe signal originated from within the brain tissue and further demonstrated a pattern of hyperpolarized ^{129}Xe distribution throughout the brain with varying signal intensity in different brain regions.

Three of the six animals studied received a vehicle injection (saline) to the left forepaw immediately prior to the acquisition of the baseline image. 10 minutes after acquisition of the baseline hyperpolarized ^{129}Xe MRS, the animal's right forepaw was injected with the chemical irritant capsaicin (20 ml of 3 mg/ml), and a second hyperpolarized ^{129}Xe spectroscopic image was acquired. Responses from three individual animals are shown in Figure 5. Whereas baseline images showed some hyperpolarized ^{129}Xe signal intensity in cortical and sub-cortical brain regions (Figure 5, left panel), images acquired following administration of capsaicin showed both higher hyperpolarized ^{129}Xe signal intensity and an increased area of distribution within the brain (Figure 5, right panel). Superimposition of a rat brain atlas (Figure 5a) revealed that areas of hyperpolarized ^{129}Xe signal increase occurred both bilaterally and

contralaterally in areas of the brain known to be involved in the processing of forepaw pain information, including the anterior cingulate and somatosensory cortices.
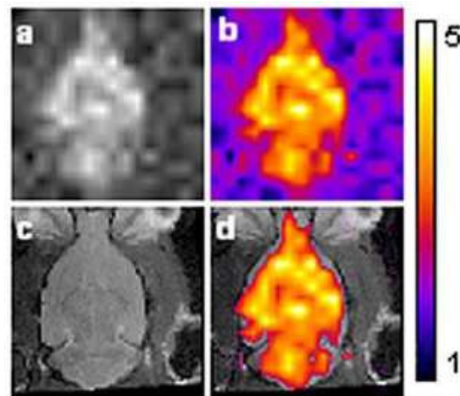

Fig. 4. Hyperpolarized ^{129}Xe signal distribution in the rat brain. (3a) hyperpolarized ^{129}Xe CSI image acquired with a 2D CSI pulse sequence from rat head under normal breathing conditions (slice thickness 10 mm). (3b) same image with false color applied. Warmer colors indicate increased hyperpolarized ^{129}Xe signal intensity. (3c) Proton MRI of a rat head showing a 1 mm coronal slice through the brain acquired with a RARE pulse sequence. (3d) Proton image shown with overlay of hyperpolarized ^{129}Xe MRI, in which only hyperpolarized ^{129}Xe signal with an SNR above 2 are shown. FOV was 25 mm.
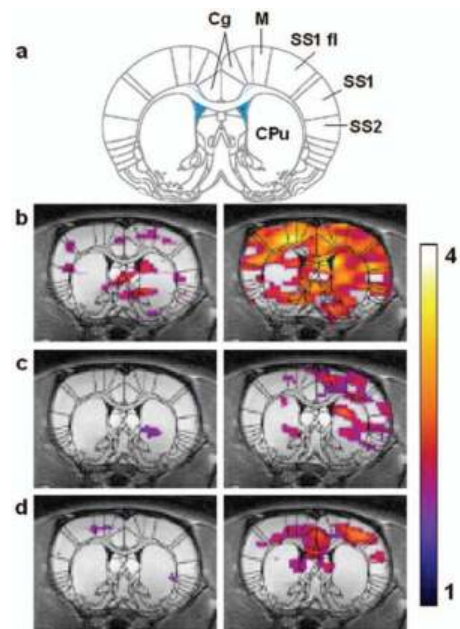
Fig. 5. Hyperpolarized ^{129}Xe fMRI data from three animals. The hyperpolarized ^{129}Xe signal is shown as a false color overlay on the corresponding 1 mm thick coronal proton reference image taken from the same animal. The left panel shows hyperpolarized ^{129}Xe signal intensity during baseline and the right panel shows hyperpolarized ^{129}Xe signal intensity after injection of capsaicin 20 ul (3 mg/ml) into the right forepaw. Color scale represents SNR and only signal with SNR above 2 are shown.

In spite of the as yet unrefined nature of this imaging modality, our results indicate that hyperpolarized [129]Xe MRI may have use as a probe for brain physiology and function. Because xenon is not inherent in the body, the substantial challenges resulting from high background signal in [1]H fMRI may be somewhat reduced. Extracting meaningful data from [1]H fMRI experiments is labour intensive, and requires a large number of subjects and image acquisitions. Extensive image post-processing is required and the influence that different post-processing steps play on the final data set achieved is actively debated. Conversely, hyperpolarized [129]Xe MRI showed patterns of brain activation consistent with those obtained using [1]H fMRI, using only a single set of images (one baseline and one post stimulus image) obtained from six animals. The magnitude of the signal difference between baseline and stimulus conditions for hyperpolarized [129]Xe (13–28%) was comparable to differences typically obtained with conventional BOLD fMRI (2 to 29%) (Bock et al., 1998; Silva et al., 1999; Mandeville et al., 1999; Tuor et al., 2000) using a rat forepaw activation paradigm.

7. Outlook of hyperpolarized [129]Xe brain MRI

This subsection will summarize the current progress as previously described, and comment the future research directions and applications in the brain imaging. Conventional MRI focuses mainly on the nuclear spin of the proton because it is ubiquitous in most parts of the human body. However, certain organs have a low proton spin density attributable to the large volume of air dispersed throughout the tissue. The low sensitivity of traditional magnetic resonance has motivated the development of techniques using hyperpolarized noble gases for NMR and MRI. Xenon has the unique characteristic of being soluble in many fluids and biological tissues, such as water, blood, lung tissue, and white and gray matter. Being a trace element in the atmosphere, xenon has no natural background signal in the human body. Therefore, dissolved-phase xenon MRI and molecular imaging could provide rich information related to biological and physiological changes beyond void space lung imaging. Efforts have demonstrated the value of dissolved xenon MRI in the study of lung gas exchange (Swanson et.al, 1999), and brain perfusion (Swanson et al., 1997; Kilian et al., 2004; Zhou et al., 2008, 2011a, 2011b) and function (Mazzanti et al., 2011). Recently, xenon-based molecular imaging has been demonstrated by using cryptophane-containing biosensors (Hilty et al., 2006). Sensitivity enhancement using a chemical amplification technique, hyperpolarized xenon chemical exchange saturation transfer (Hyper-CEST) (Schröder et al., 2006), allows imaging at low concentrations; however, for *in vivo* applications the small filling factor of a region of interest in the body relative to the NMR coil is a significant factor limiting sensitivity. In such cases remote detection methods (Hilty et.al, 2005) can provide dramatic improvements in sensitivity. In remote detection, the normal NMR coil that contains the full region of interest is used to encode spectroscopic and spatial information, then stores it as longitudinal magnetization. These encoded spins then flow into a second coil with an optimized filling factor for detection.

Remote detection can overcome the filling factor issue of dissolved xenon MRI, although a low concentration of xenon in solution can be another significant impediment to highly sensitive detection. It has been shown that the solvated xenon signal can be amplified by xenon polarization transfer contrast, in which the dissolved-phase xenon from either lungs or brains is selectively saturated, and through exchange, the gas-phase signal is attenuated.

This method is able to indirectly image dissolved-phase xenon, but is limited to tissue in direct exchange with the air in the lungs. The gas exchange process could be similarly exploited for direct signal amplification of dissolved xenon with the remote detection technique, which extends the study area from lung to brain. Xenon gas can be extracted from the dissolved solutions and concentrated in the gas phase for detection. Furthermore, with the long longitudinal relaxation time of gas-phase xenon, extracted xenon gas from solution can be compressed or liquefied while preserving the encoded information. The xenon density in the liquid state is approximately four orders of magnitude higher than in aqueous solutions, which in principle could result in up to 10,000 times enhancement of spin density, thus allowing substantial signal amplification

We have demonstrated the hyperpolarized xenon signal amplification by gas extraction (Hyper-SAGE) method (Zhou et al., 2009b) with enhanced NMR spectra and time-of-flight (TOF) images by using recently commercialized membrane technology for high-efficiency xenon dissolution (Baumer et.al, 2006). The Hyper-SAGE technique relies on physical amplification by exploiting a phase change and is completely distinct from chemical amplification. In combination with additional amplification techniques such as Hyper-CEST, this method promises to dramatically decrease the detection threshold of MRI and has the potential to benefit molecular imaging applications and brain imaging.

Recent innovations in the production of highly polarized [129]Xe and novel method of signal enhancement should make feasible the emergence of hyperpolarized [129]Xe MRI as a viable adjunct method to conventional MRI for the study of brain function and disease. The high sensitivity of hyperpolarized noble gas signal and non-background noise in biological tissue offer xenon as an important and promising contrast agent to study the brain. Because the polarization of hyperpolarized xenon does not depend on the magnetic field strength, the technique for brain imaging could also be applied for use with low field portable MRI devices (Appelt, 2007; Blümich, 2008; Paulsen, 2008).

8. Acknowledgments

9. References

Albert MS, et al. (1994). Biological magnetic resonance imaging using laser-polarized [129]Xe. *Nature*, Vol. 370, pp.(199–201).

Andrea & Angelo (2003), Hyperpolarised xenon in biology. *Nucl. Magn. Reson. Spectr.*, Vol. 4, pp.(1–30).

Appelt S, et al. (2005). Mobile high-resolution xenon nuclear magnetic resonance spectroscopy in the Earth's magnetic field. *Phys Rev Lett*, Vol.94, pp.(197602).

Baumer D, et al. (2006). NMR spectroscopy of laser-polarized [129]Xe under continuous flow: A method to study aqueous solutions of biomolecules. *Angew Chem Int Ed*, Vol. 45, pp.(7282–7284).

Betz E .(1972). Cerebral blood flow: Its measurement and regulation. *Physiol. Rev.*, Vol. 52: 595–630

Bock C, et al. (1998). Functional MRI of somatosensory activation in rat: effect of hypercapnic upregulation on perfusion- and BOLD-imaging. *Magn. Reson. Med.*, Vol. 39, pp.(457–461).

Blümich B, et al. (2008). Mobile single-sided NMR. *Prog. Nucl. Magn. Reson. Spectr.*, Vol.52, pp.(197–269).

Cherubini A & Bifone A. (2003). Hyperpolarized xenon in biology. *Prog. Nucl. Magn. Reson. Spectr.*, Vol. 42, pp.(1–30).

Choquet P, et al. (2003) Method to determine *in vivo* the relaxation time T1 of hyperpolarized xenon in rat brain. *Magn. Reson. Med.*, Vol. 49, pp.(1014–1018).

Cook GE. (1961). Argon, Helium and the Rare Gases, Interscience Publishers, New York

Duhamel G, et al. (2000). *In vivo* ^{129}Xe NMR in rat brain during intra-arterial injections of hyperpolarized ^{129}Xe dissolved in a lipid emulsion. *C.R. Acad. Sci. III*, Vol. 323, pp. (529-536).

Duhamel G, et al. (2002). Global and regional cerebral blood flow measurements using NMR of injected hyperpolarized xenon-129. *Acad. Radiol.*, Vol. suppl 2, pp.(S498-S500).

Goodson BM. (2002). Nuclear magnetic resonance of laser-polarized noble gases in molecules, materials, and organisms. *J. Magn. Reson.*, Vol.155, pp.(157–216).

Gur D & Good WF.(1982). *In vivo* mapping of local cerebral blood flow by xenon-enhanced computed tomography. *Science,* Vol.215, pp.(1267–1268).

Hilty C, et al. (2006). Spectrally resolved magnetic resonance imaging of a xenon biosensor. *Angew. Chem. Int. Ed.* Vol.45, pp.(70–73).

Hilty C, et al. (2005). Microfluidic gas-flow profiling using remote-detection NMR. *Proc. Natl. Acad. Sci. USA*, Vol.102, pp.(14960–14963).

Kilian W, et al. (2004). Dynamic NMR spectroscopy of hyperpolarized ^{129}Xe in human brain analyzed by an uptake model. *Magn. Reson. Med.*, Vol. 51, pp.(843–847).

Mandeville JB, et al. (1999). MRI measurement of the temporal evolution of relative CMRO2 during rat forepaw stimulation. *Magn. Reson. Med.*, Vol. 42, pp.(944–951).

Martin CC, et al. (1997). The pharmacokinetics of hyperpolarized xenon: implications for cerebral MRI. *J. Magn. Reson. Imag.*, Vol. 7, pp.(848–854).

Mazzanti M, et al. (2011). Distribution of hyperpolarized xenon in the brain following sensory stimulation: preliminary MRI findings. *PLoS ONE*, Vol. 6, pp.(e21607).

Meng X, et al. (2004). Characterizing the diffusion/perfusion mismatch in experimental focal cerebral ischemia. *Ann. Neurol.*, Vol. 55, pp.(207-212).

Navon et al. (1996). Enhancement of solution NMR and MRI with laser-polarized xenon. *Science*, Vol. 271, pp.(1848-1851).

Oros A-M & Shah NJ. (2004). Hyperpolarized xenon in NMR and MRI. *Phys. Med. Biol.*, Vol. 49, pp.(R105–R153).

Paulsen JL, et al. (2008). Volume-selective magnetic resonance imaging using an adjustable, single-sided, portable sensor. *Proc. Natl. Acad. Sci. USA*, Vol.105, pp.(20601–20604).

Peled S, et al. (1996). Determinants of tissue delivery for ^{129}Xe magnetic resonance in humans. *Magn. Reson. Med.*, Vol. 36, pp.(340–344).

Ruppert K, et al. (2000). Probing lung physiology with xenon polarization transfer contrast (XTC). *Magn. Reson. Med.*, Vol. 44, pp.(349–357).

Swanson SD & Rosen MS. (1997). Brain MRI with laser-polarized ^{129}Xe. *Magn. Reson. Med.*, Vol.38, pp.695–698,

Swanson SD & Rosen MS. (1999). Distribution and dynamics of laser-polarized ^{129}Xe agnetization *in viv*o. *Magn. Reson. Med.,* 42:1137–1145.

Saam BT, et al. (2000). MR imaging of diffusion of ^{3}He gas in healthy and diseased lungs. *Magn. Reson. Med.,* Vol.44, pp.(174–179).

Schöder L, et al. (2006). Molecular imaging using a targeted magnetic resonance hyperpolarized biosensor. *Science,* Vol. 314, pp.(446–449).

Silva AC, et al. (1999). Simultaneous blood oxygenation level-dependent and cerebral blood flow functional magnetic resonance imaging during forepaw stimulation in the rat. *J. Cereb. Blood. F. Met.*, Vol. 19, pp.(871–879).

Tuor UI, et al. (2000). Functional magnetic resonance imaging in rats subjected to intense electrical and noxious chemical stimulation of the forepaw. *Pain*, Vol. 87, pp.(315–324).

Walker TG & Happer W. (1997). Spin-exchange optical pumping of noble-gas nuclei. *Rev. Mod. Phys.*, Vol. 69, pp.(629–642).

Wakai A, et al. (2005). A method for measuring the decay time of hyperpolarized ^{129}Xe magnetization in rat brain without estimation of RF flip angles. *Magn. Reson. Med. Sci.*, Vol. 4, pp.(19–25).

Wilson GJ, et al. (1999). Longitudinal relaxation times of ^{129}Xe in rat tissue homogenates at 9.4 T. *Magn. Reson. Med.*, Vol. 41, pp.(933–938).

Zhou X, et al. (2004a). Production of Hyerpolarized ^{129}Xe Gas without Nitrogen by Optical Pumping at ^{133}Cs D_2 Line in Flow System. *Chin. Phys. Lett.*, Vol.21, pp.(1501-1503).

Zhou X, et al. (2004b). Experimental and Dynamic Simulations of Radiation Damping of Laserpolarized Liquid ^{129}Xe at Low Magnetic Field in a Flow System. *Appl. Magn. Reson.*, Vol. 26, pp.(327-337).

Zhou X, et al. (2004c). Enhancement of Solid-state Proton NMR via SPINOE with Laser-polarized Xenon. *Phys. Rev. B,* Vol. 70, pp.(052405-1-052405-4).

Zhou X, et al. (2008). Reinvestigating Hyperpolarized ^{129}Xe Longitudinal Relaxation Time in the Rat Brain with Noise Considerations. *NMR in Biomedicine*, Vol.21, pp.(217-225).

Zhou X. et al. (2009a). Quantitative Estimation of SPINOE Enhancement in Solid State. *J. Magn. Reson.*, Vol. 196, pp.(200-203).

Zhou X, et al. (2009b). Hyperpolarized Xenon NMR and MRI Signal Amplification by Gas Extraction. *Proc. Natl. Acad. Sci. USA*, Vol.106, pp.(16903-16906).

Zhou X, et al. (2011a). MRI of Stroke using Hyperpolarized ^{129}Xe. *NMR in Biomedicine*, Vol. 24, pp.(170-175).

Zhou X, et al. (2011b). Distribution of Hyperpolarized Xenon in the Brain Following Sensory Stimulation: Preliminary MRI Findings. *PLoS ONE*, Vol. 6, pp.(e21607).

Zhou X, et al. (2011c). Hyperpolarized ^{129}Xe magnetic resonance imaging and its applications in biomedicine. *Physics* (review article in Chinese), Vol. 40, pp.(379-388).

http://science.nasa.gov/science-news/science-at-nasa/2008/25apr_cvx2/
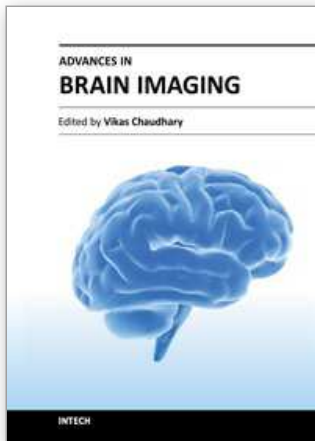
Advances in Brain Imaging
Edited by Dr. Vikas Chaudhary

Remarkable advances in medical diagnostic imaging have been made during the past few decades. The development of new imaging techniques and continuous improvements in the display of digital images have opened new horizons in the study of brain anatomy and pathology. The field of brain imaging has now become a fast-moving, demanding and exciting multidisciplinary activity. I hope that this textbook will be useful to students and clinicians in the field of neuroscience, in understanding the fundamentals of advances in brain imaging.

How to reference

In order to correctly reference this scholarly work, feel free to copy and paste the following:

Xin Zhou (2012). Hyperpolarized Xenon Brain MRI, Advances in Brain Imaging, Dr. Vikas Chaudhary (Ed.), ISBN: 978-953-307-955-4, InTech, Available from: http://www.intechopen.com/books/advances-in-brain-imaging/hyperpolarized-xenon-brain-mri

INTECH
open science | open minds